M. L. ZHANG
Y. D. ZHANG
M. JI
and
H. J. GUO

Estimation of tunnel stability and optimization of support parameters for tunnel below gob pillar in closely-spaced coal seams

After the upper coal seam mining, stress concentrations under the residual pillar generate an inhomogeneous stress field and the stress on the tunnel increases. This can lead to tunnel destruction if the external forces exceed the strength of the composite rock–bolt bearing structure (CRBBS). The Weibull distribution function was introduced to modify the calculation formula of the CRBBS strength and stress distribution of the CRBBS. The radial stress within the CRBBS under the inhomogeneous stress field was calculated. The tunnel instability coefficient (η) was derived to quantitatively describe the relationship among the tunnel position, tunnel parameters, support parameters, and rock mechanical properties. The coefficient is the ratio of the maximum radial stress within CRBBS to the CRBBS strength; the CRBBS is stable only when η<1. The instability coefficient of the 21178 return tunnel Huopu colliery was calculated to obtain the optimised support parameters.The bolt strength was adjusted from 335MPa to 500MPa and the bolt length was changed from 2.2m to 2.5m; thus, the large deformation of the 21178 return tunnel was controlled. The optimum distance between the 21178 return tunnel and the pillar edge was at least 12.4m. The proposed method was validated by comparison with results by the tunnel stability index method (>20m), abutment pressure influence edge method (14.6m), and rateo fstress change method (>16.2m). Since the resistance of the bolt support is quantified, the tunnel position evaluated by the tunnel instability coefficient is more practical.

Keywords: *Gob pillar; CRBBS; tunnel instability coefficient; optimization of support parameters; tunnel position*

1 Introduction

In many mining areas in China, such as the Datong, Jinglong, Pingdingshan, and Handan areas, mining of closely-spaced coal seams (CSCS) is common; in CSCS the seam separation is less than or equal to the depth of the floor damage zone formed during the mining of the upper coal seam (Kang et al.,2011, Tan et al., 2010). In the past few years, high-intensity mining enabled by the development of highly efficient and highly productive mining techniques have exhausted many of the easily exploitable underground coal deposits. This has greatly increased the importance of CSCS (Li et al., 2005, Zhao et al., 1998).

One of the most common and complex problems in CSCS mining is the stress distribution under the upper gob pillar as well as the position and support for the tunnel; these issues have been studied extensively. Wilson (1983) proposed a method to help design underground structures such as tunnels, face supports, and pillars in coal mines. This method was tested in a number of mines. Lu et al. (1993) used a coefficient, derived from regression analysis of many field projects, to evaluate the stability of tunnel–pillar distances. Suchowerska et al.(2013) examined the factors that affect the magnitude and distribution of the pressure below the gob pillars. Liuet al. (2016) presented a numerical simulation of the stress distribution of the lower seams below a pillar and the diffusion angle of the pillar floor. Fang et al.(2016) used tests on a scaled model to analyse the displacement and stresses in the rocks surrounding a highway tunnel adjacent to an overlying mined-out thin coal seam and evaluated the stability control methods. Mathey and Merwe (2016) analysed the calculation of pillar strength and established an effective narrow-reef platinum mining pillar design systems of the south African. Yan et al. (2015) conducted simulations on the support effect of several support parameters and tunnel positions. The conclusions reached by that study provided guidance for tunnel position and support design in the lower coal seam. In a theoretical study of tunnel position and design, Zhang et al. (2012) discovered that a tunnel located in a heterogeneous stress field formed by the upper coal seam pillar was more prone to damage than a tunnel in a uniform stress field. Xie et al. (2016) analyzed the breaking and forming process of distinguishing key block structures in close spaced coal seams and established an integrated mechanical model of distinguishing structures.

Messrs. M.L. Zhang, M. Ji, H. J. Guo, School of Mines, Key Laboratory of Deep Coal Resource Mining, Ministry of Education of China; China University of Mining & Technology and Y. D. Zhang, State Key Laboratory of Coal Resources and Safe Mining, School of Mines; China University of Mining & Technology, Corresponding author: e-mail: jiming@cumt.edu.cn

In summary, many studies drew meaningful conclusions in relation to the stress distribution below the upper gob pillar as well as the tunnel position and support. However, much of the research in this area has been on tunnels without supporting structures and on tunnels driven outside the gob-pillar stress field. Such studies neglect the effect of the bolt support on the mechanics and the position of the tunnel. Moreover, the tunnels defined by traditional methods are commonly located outside the gob-pillar edge, which means that the cost of resources incurred by the wider gob pillar is not evaluated. Where tunnels have to be driven in areas influenced by gob-pillar stress, suitable support methods must be used to ensure their safety. Consequently, quantitative research on the relationships between the pillar dimensions, tunnel position, tunnel support parameters, and tunnel stability can have extremely important implications for tunnel safety in CSCS. Accordingly, in this study the tunnel and bolts were considered as a whole unit to quantitatively analyse the relationship among the tunnel position, tunnel parameters, support parameters, and rock mechanical properties. Using this method on a coal mine case study, the bolt array pitch was optimized and the severe deformation in the return tunnel was alleviated.

2. Calculation theory

After tunnel excavation, bolts with suitable preload are installed in the surrounding rock to maintain the tunnel stability. For a circular tunnel, multiple bolts of appropriate length are installed in the tunnel wall; by incorporating the bolts into the surrounding rock, a unified structure, the composite rock-bolt bearing structure (CRBBS) as expressed in Fig.1 is formed. The CRBBS is homogeneous in the circles of broken rock around the tunnel formed by tunnel excavation. The support of the bolts for the inner surface of the tunnel is uniformly distributed.

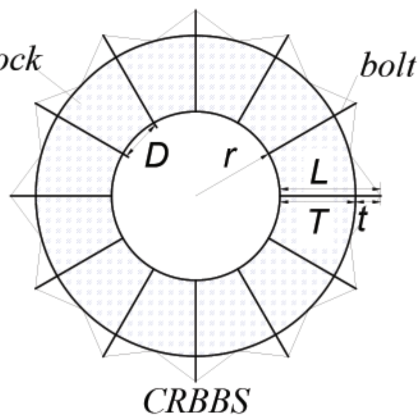

Fig.1 Illustration of CRBBS cross section

The Breakthrough-point theory proposed by Yang et al. (2013) and Shanget al. (2014) states that the destruction of a structure originates from one or several specific points where the stress within the rock mass reaches or exceeds the strength of the surrounding rock. In the destruction of a CRBBS, the unified bearing ability of a rock–bolt structure should be considered rather than solely the rock damage. A homogeneous CRBBS follows the Mohr-Coulomb yield criterion and the surrounding rock is an isotropic homogeneous plane strain medium without any creep or viscosity. In a CRBBS, as shown in Fig.2, the stress in the surrounding rock and the cohesion and internal friction angle of the bearing structure is improved by the bolts (Hou, 2013). This is aided by the strength envelope of the surrounding rock shifting from line a to line b. The vertical stress, σ_1, and the horizontal stress, σ_3, at any point in the CRBBS will change with any perturbation caused by an external force. As the radius of the Mohr stress circle of the CRBBS increases with increasing vertical stress or decreasing horizontal stress, the destruction of the CRBBS will occurs once the Mohr stress circle reaches the strength envelope of the CRBBS.

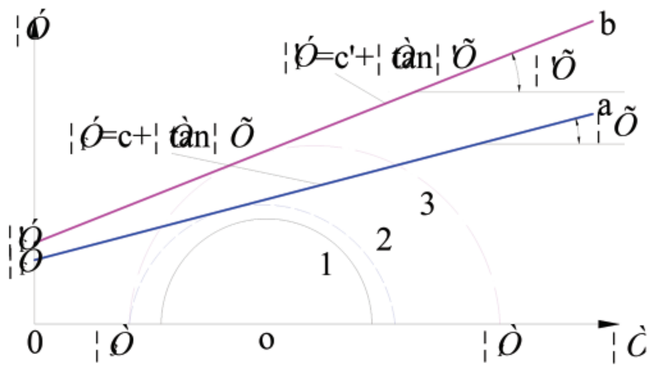

Fig.2 Stress and strength in a CRBBS
(a is the strength curve of the rock and b is the strength curve of the CRBBS)

Fig.3 shows the inhomogeneous stress field (σ_p) caused by stress distribution below the pillar that remains after the upper coal seam has been mined. The load under the pillar gradually decreases as the tunnel–pillar distance increases and the vertical stress in the floor strata also decreases. Analogous to tunnels under asymmetrical loading, the stress within the CRBBS would increase unevenly in this heterogeneous stress field and this would probably damage

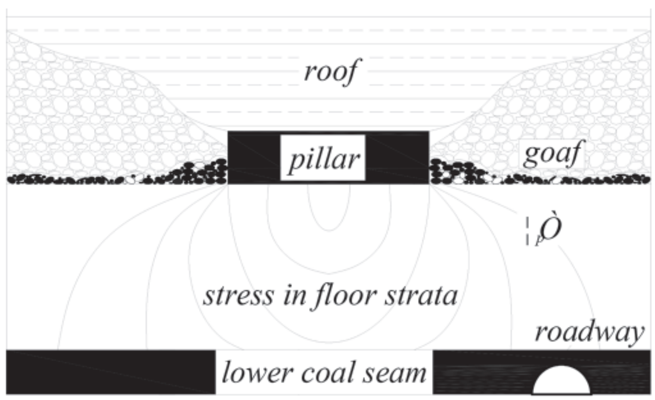

Fig.3 Layout of a tunnel in closely-spaced coal seams

the tunnel support structure located in the rock stratum below the upper gob pillar or in the lower coal seam (Yang et al., 2015). Accordingly, in a tunnel below a gob pillar, the CRBBS is subjected to increased stress caused by the inhomogeneous stress field; once the stress within the CRBBS reaches or exceeds the ultimate strength of the CRBBS the tunnel will collapse. The strength of the CRBBS is influenced by the physical and mechanical characteristics of the surrounding rock, the tunnel size, and the support parameters. The maximum radial stress within the CRBBS is determined mainly by the load on the gob pillar, the position of the tunnel, and the support parameters. If the strength of the CRBBS is larger than the maximum radial stress within the CRBBS, the CRBBS will remain stable and safe.

2.1 CRBBS geometry and stress distribution

(1) CRBBS geometric parameters

As illustrated in Fig.1, a number of bolts, μ, are emplaced in each semi-circular tunnel section. The bolt interval can be expressed as

$$D_a = \frac{\pi r}{\mu - 1} \quad \text{... (1)}$$

where D_a is the bolt interval and r is the radius of the tunnel.

Equation (2) describes the radial thickness of the CRBBS:

$$T = L - t = L - \frac{\pi(r+L)}{2(\mu-1)} \quad \text{... (2)}$$

where T is the thickness of the CRBBS, L is the length of the bolt, and t ($t = \frac{(\mathrm{r+L})\mathrm{D}}{r \quad 2}$) is the thickness of the conical compression zone around the bolt head.

The supporting strength of the bolts can be expressed as

$$P_i = \frac{\mu\pi d^2 \sigma_b (\mu - 1)}{4\pi r D_b} \quad \text{... (3)}$$

where P_i is the supporting strength of the bolts, D_a is the array pitch of the bolt, d is the bolt diameter, and σ_b is the tensile strength of the bolt.

(2) Calculation of CRBBS strength

A mechanical analysis based on half of the CRBBS is shown in Fig.4; the CRBBS is subjected to a vertical force and to the homogeneous stress field, and is supported by the underlying strata (Cheng et al., 2015). Assuming that F_w is the vertical force supporting the tunnel, F_q is the vertical component of the force overlying the CRBBS, and F_b is the radial force of the bolt support. Because the external force on the CRBBS can achieve horizontal self-balance, a necessary condition to balance the external force is the equilibrium of the vertical forces. This can be expressed as

$$2F_w = F_q + F_b \quad \text{... (4)}$$

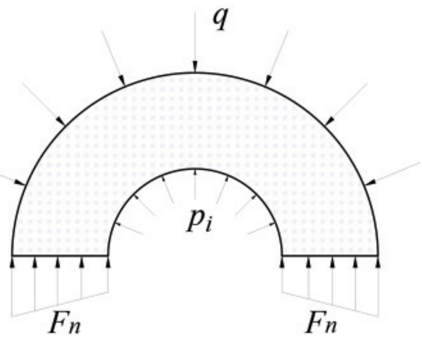

Fig.4 Mechanical model for composite rock-bolt bearing structure

The expressions for F_w, F_q, and F_b can be written as

$$F_w = \int_0^T \left\{ \left[p_i + f(x) \right] \frac{1+\sin\varphi}{1-\sin\varphi} + \frac{2c\cos\varphi}{1-\sin\varphi} \right\} dx \quad \text{... (5)}$$

$$F_q = \int_0^\pi p_i r \sin\alpha \, d\alpha \quad \text{... (6)}$$

$$F_b = \int_0^\pi q(r+T) \sin\alpha \, d\alpha \quad \text{... (7)}$$

where $f(x)$ is a distribution function describing the increment of the radial stress along the CRBBS cross section, and x is the distance from a certain point to the tunnel surface along the CRBBS cross section. Substituting Eq. (5), (6), and (7) into Eq. (4) we obtain

$$2\int_0^T \left\{ \left[p_i + f(x) \right] \frac{1+\sin\varphi}{1-\sin\varphi} + \frac{2c\cos\varphi}{1-\sin\varphi} \right\} dx = \int_0^\pi q(r+T)\sin\alpha \, d\alpha - \int_0^\pi p_i r \sin\alpha \, d\alpha \quad \text{... (8)}$$

The strength of the CRBBS can be expressed as (Cheng, 2015) :

$$q = \frac{L - \frac{\pi(r+L)}{2(\mu-1)}}{r + L - \frac{\pi(r+L)}{2(\mu-1)}} \left\{ \left[\frac{\mu\pi d^2\sigma_b(\mu-1)}{4\pi r D_b} + \frac{1}{2} a \left(L - \frac{\pi(r+L)}{2(\mu-1)} \right) \right] \frac{1+\sin\varphi}{1-\sin\varphi} + \frac{2c\cos\varphi}{1-\sin\varphi} + \frac{\mu\pi d^2\sigma_b(\mu-1)}{4\pi r D_b} \times \frac{r}{L - \frac{\pi(r+L)}{2(\mu-1)}} \right\} \quad \text{...9}$$

where c is the rock cohesion (MPa), φ is the rock internal friction angle, and α is a coefficient defined by the hydrostatic pressure.

In the literature (Cheng et al., 2015) the radial stress is defined as $f(x)=ax$ which is a simplified representation of the actual situation; therefore, a more accurate function, the Weibull distribution function, is introduced to describe the strength of the CRBBS. Previous work showed that when $x<x_c$ in the Weibull distribution function the increment of the

vertical stress along the CRBBS cross section can be described as

$$g(x)=E_0 x e^{-\frac{x}{x_c}} \quad \text{... (10)}$$

where E_0 is the initial slope of $g(x)$.

The derivative of Eq.(10) can be expressed as

$$g'(x)=E_0\left(1-x/x_c\right)e^{-\frac{x}{x_c}} \quad \text{... (11)}$$

Let $g'(x) = 0$; if $x = x_c$, $g(x) = g_c$ (g_c is at the peak value), then E_0 can be written as $E_0 = g_c e/x_c$. For the stress distribution in the rock, x_c is the boundary of the initial stress and g_c is the initial stress.

Then Eq.(11) can be expressed as

$$g(x)=\frac{g_c e}{x_c} x e^{-\frac{x}{x_c}} \quad \text{... (12)}$$

Equation (12) is illustrated in Fig.5. According to Fig.4 and Eq.(9), the peak value of $g(x)$ depends on g_c and the slope of $g(x)$ can be adjusted by x_c.

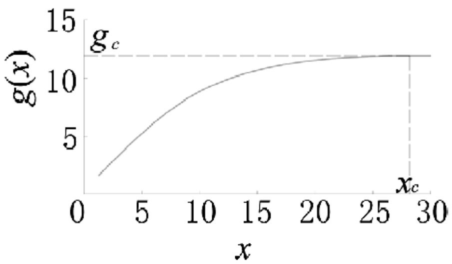

Fig.5 Weibull distribution function (for x < xc)

Based on the radial stress distribution of the surrounding rock, the increment of the radial stress can be expressed as

$$g(x)=e\left(\sigma_{\rho\text{原}}-p_i\right)\frac{x}{x_c}e^{-\frac{x}{x_c}} \quad \text{... (13)}$$

Homogeneous rock supported by bolts follows the Mohr-Coulomb yield criterion. Substituting Eq.(13) into the Mohr-Coulomb yield criterion we obtain

$$f(x)=\sigma_\theta=e\frac{1+\sin\varphi}{1-\sin\varphi}\left(\sigma_{\rho\text{原}}-p_i\right)\frac{x}{x_c}e^{-\frac{x}{x_c}}+2c\cos\varphi \quad \text{... (14)}$$

Substituting Eq.(14) into Eq.(8) yields

$$q=\frac{T\left[\left(p_i+\int_0^T\left(e\frac{1+\sin\varphi}{1-\sin\varphi}\left(\sigma_{\rho\text{原}}-p_i\right)\frac{x}{x_c}e^{-\frac{x}{x_c}}+2c\cos\varphi\right)\right)\frac{1+\sin\varphi}{1-\sin\varphi}+\frac{2c\cos\varphi}{1-\sin\varphi}\right]+rp_i}{r+T} \quad \text{... (15)}$$

Applying an integral algorithm to Eq.(15) we can obtain

$$q=\frac{L-\frac{\pi(r+L)}{2(\mu-1)}}{r+L-\frac{\pi(r+L)}{2(\mu-1)}}\left\{\begin{aligned}&\left[\frac{\mu\pi d^2\sigma_b(\mu-1)}{4\pi rD_b}+\left(\begin{aligned}&e\frac{1+\sin\varphi}{1-\sin\varphi}\left(\sigma_{\rho\text{原}}-\frac{\mu\pi d^2\sigma_b(\mu-1)}{4\pi rD_b}\right)\\&\left\{x_c-\left(x_c+L-\frac{\pi(r+L)}{2(\mu-1)}\right)e^{-\frac{L-\frac{\pi(r+L)}{2(\mu-1)}}{x_c}}\right\}+2c\cos\varphi\end{aligned}\right)\right]\frac{1+\sin\varphi}{1-\sin\varphi}\\&+\frac{2c\cos\varphi}{1-\sin\varphi}+\frac{\mu\pi d^2\sigma_b(\mu-1)}{4\pi rD_b}\times\frac{r}{L-\frac{\pi(r+L)}{2(\mu-1)}}\end{aligned}\right\} \quad \text{... (16)}$$

(3) Stress distribution within the CRBBS

The limit stress of a certain point within the CRBBS under hydrostatic pressure can be expressed by

$$\begin{cases}\sigma'_\rho=\frac{\mu\pi d^2\sigma_b(\mu-1)}{4\pi rD_b}+e\frac{1+\sin\varphi}{1-\sin\varphi}\left(\sigma_{\rho\text{原}}-\frac{\mu\pi d^2\sigma_b(\mu-1)}{4\pi rD_b}\right)\frac{\rho}{x_c}e^{-\frac{\rho}{x_c}}+2c\cos\varphi\\ \sigma'_\theta=\left(\frac{\mu\pi d^2\sigma_b(\mu-1)}{4\pi rD_b}+e\frac{1+\sin\varphi}{1-\sin\varphi}\left(\sigma_{\rho\text{原}}-\frac{\mu\pi d^2\sigma_b(\mu-1)}{4\pi rD_b}\right)\frac{\rho}{x_c}e^{-\frac{\rho}{x_c}}+2c\cos\varphi\right)\frac{1+\sin\varphi}{1-\sin\varphi}+\frac{2c\cos\varphi}{1-\sin\varphi}\end{cases} \quad \text{... (17)}$$

where ρ is the radial distance between the point and the origin of the polar coordinates (OPC), and θ is the angle between the horizontal line to the left of the OPC and the line connecting the point and the OPC in a clockwise direction.

2.2 Additional stress on the gob pillar

As reported in previous studies, the stress in the gob pillar is affected by the pillar width, burial depth, mining height, abutment pressure imposed by the mining, and other factors. (Yan et al., 2015, Yang et al., 2015). The characteristic bearing curve was approximated using a three-section liner to estimate the load on the gob pillar, as illustrated in Fig.6.

The stress on the gob pillar can be expressed as

$$q_p=\frac{K_1x_1+(K_1+K_2)x_2+2K_2x_3+(K_2+K_3)x_4+K_3x_5}{2x_p}\gamma H \quad \text{... (18)}$$

where q_p is the uniform load on the pillar; H is the depth of burial; K_1, K_2, and K_3 are multiples of the initial rock stresses; γ is the average bulk density of the overlying strata; x_1, x_2, x_3, x_4, and x_5 are the lengths of the five stress stages; x_p is the width of the pillar.

In rectangular coordinates with the origin at P(0, 0) (the centre of the gob pillar), the additional radial and tangential stresses imposed by the load on the gob pillar are designated as σ^P and τ^P. In polar coordinates with the origin at R(j, k) (the centre of the tunnel), the radial and tangential stresses are designated as σ^R and τ^R. Using this notation, the stress at any point in the gob pillar floor can be expressed by Eq. (19):

$$
\begin{cases}
\sigma^{P}{}_{x} = \dfrac{q_p}{\pi}\left[\arctan\dfrac{z+x_p/2}{z} - \arctan\dfrac{x-x_p/2}{z} - \dfrac{z(x+x_p/2)}{z^2+(x+x_p/2)^2} + \dfrac{z(x-x_p/2)}{z^2+(x-x_p/2)^2}\right] \\
\sigma^{P}{}_{z} = \dfrac{q_p}{\pi}\left[\arctan\dfrac{x+x_p/2}{z} - \arctan\dfrac{x-x_p/2}{z} + \dfrac{z(x+x_p/2)}{z^2+(x+x_p/2)^2} - \dfrac{z(x-x_p/2)}{z^2+(x-x_p/2)^2}\right] \\
\tau^{P}{}_{xz} = -\dfrac{q_p}{\pi}\left[\dfrac{z^2}{z^2+(x+x_p/2)^2} - \dfrac{z^2}{z^2+(x-x_p/2)^2}\right]
\end{cases} \quad \text{... (19)}
$$

Assuming that the tunnel is located below the lower right part of the gob pillar, the maximum stress on the CRBBS would be in the left semi-circle in Fig.4. The rectangular and polar coordinates can be transformed using Eq. (20) and the stresses can be expressed in polar coordinates as Eq. (21).

$$
\begin{cases}
x = j - \rho\cos\theta \\
y = k - \rho\sin\theta
\end{cases} \quad \text{... (20)}
$$

$$
\begin{cases}
\sigma^{P}{}_{j-\rho\cos\theta} = \dfrac{q_p}{\pi}\left[\begin{array}{l} \arctan\dfrac{k-\rho\sin\theta+x_p/2}{k-\rho\sin\theta} - \dfrac{(k-\rho\sin\theta)(j-\rho\cos\theta+x_p/2)}{(k-\rho\sin\theta)^2+(j-\rho\cos\theta+x_p/2)^2} \\ -\arctan\dfrac{x-x_p/2}{k-\rho\sin\theta} + \dfrac{(k-\rho\sin\theta)(j-\rho\cos\theta-x_p/2)}{(k-\rho\sin\theta)^2+(j-\rho\cos\theta-x_p/2)^2} \end{array}\right] \\
\sigma^{P}{}_{k-\rho\sin\theta} = \dfrac{q_p}{\pi}\left[\begin{array}{l} \arctan\dfrac{j-\rho\cos\theta+x_p/2}{k-\rho\sin\theta} + \dfrac{(k-\rho\sin\theta)(j-\rho\cos\theta+x_p/2)}{(k-\rho\sin\theta)^2+(j-\rho\cos\theta+x_p/2)^2} \\ -\arctan\dfrac{j-\rho\cos\theta-x_p/2}{k-\rho\sin\theta} - \dfrac{(k-\rho\sin\theta)(j-\rho\cos\theta-x_p/2)}{(k-\rho\sin\theta)^2+(j-\rho\cos\theta-x_p/2)^2} \end{array}\right] \\
\tau^{P}{}_{(j-\rho\cos\theta)(k-\rho\sin\theta)} = -\dfrac{q_p}{\pi}\left[\begin{array}{l} \dfrac{(k-\rho\sin\theta)^2}{(k-\rho\sin\theta)^2+(j-\rho\cos\theta+x_p/2)^2} \\ -\dfrac{(k-\rho\sin\theta)^2}{(k-\rho\sin\theta)^2+(j-\rho\cos\theta-x_p/2)^2} \end{array}\right]
\end{cases} \quad \text{... (21)}
$$

In polar coordinates with the origin at R (j, k), the centre of the tunnel, the radial stress can be described by:

$$
\begin{cases}
\sigma''_{\rho} = \sigma^{P}{}_{j-\rho\cos\theta}\cos^2\theta + \sigma^{P}{}_{k-\rho\sin\theta}\sin^2\theta + 2\tau^{P}{}_{(j-\rho\cos\theta)(k-\rho\sin\theta)}\sin\theta\cos\theta \\
\sigma''_{\theta} = \sigma^{P}{}_{j-\rho\cos\theta}\sin^2\theta + \sigma^{P}{}_{k-\rho\sin\theta}\cos^2\theta - 2\tau^{P}{}_{(j-\rho\cos\theta)(k-\rho\sin\theta)}\sin\theta\cos\theta
\end{cases} \quad \text{... (22)}
$$

2.3 Tunnel instability coefficient

According to the calculations presented in previous sections, the stress at any point within the CRBBS can be expressed as

$$
\begin{cases}
\sigma^{R}{}_{\rho} = \sigma'_{\rho} + \sigma''_{\rho} \\
\sigma^{R}{}_{\theta} = \sigma'_{\theta} + \sigma''_{\theta}
\end{cases} \quad \text{... (23)}
$$

and the radial stress on the surface of the CRBBS can be represented by

$$
\sigma_T = \sigma^{R}{}_{\rho}\Big|_{\rho=T} \quad \text{... (24)}
$$

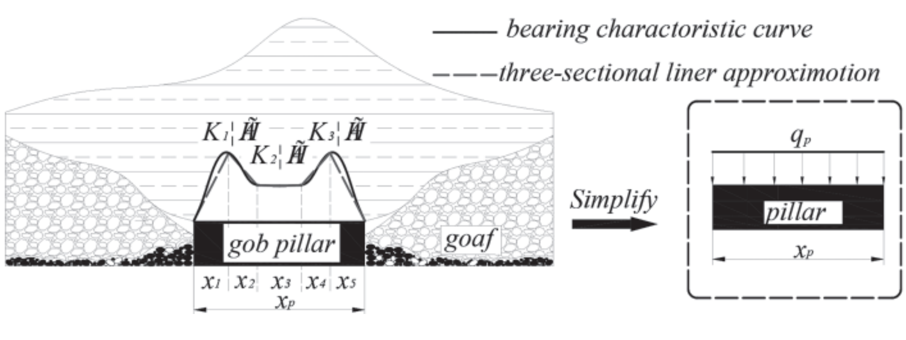

Fig.6 Diagram showing the load distribution on a pillar

When the maximum radial stress σ_{Tmax} is less than the strength of the CRBBS, the CRBBS will remain stable. If this is not the case, the CRBBS will collapse. A safety factor (Cheng et al., 2003), with a range of 1-2, is introduced to ensure the integrity of the CRBBS.This factor is reflected in Eq. (25):

$$q \geq n\sigma_{T\max} \quad \text{... (25)}$$

The tunnel instability coefficient, η, can be defined as

$$\eta = \frac{n\sigma_{T\max}}{q} \quad \text{... (26)}$$

After substituting Eqs. (16), (17), and (22) into Eq. (26), the tunnel instability coefficient can be solved.

The tunnel remains intact if η >1. The relationships among the pillar dimensions, tunnel position, tunnel support parameters, and tunnel stability are determined by Eq. (26). After the parameters are assigned according to the simulation, the tunnel's position can be determined, the CRBBS can be designed, and the tunnel's stability can be predicted.

3. Study case

3.1 General background of the study site

The Huopu colliery is located in Guizhou Province, China. There are five workable coal seams: #3, #7, #12, #14, and #17. The thickness of coal seams#14 and #17are 3.75m and 6m, respectively. with a 14.1-m-thick clayey siltstone layer between them (Fig.7). Working face 21178 is in coal seam #17 and is buried 484m underground. Working faces 21145 and 21146 in coal seam #14 have been mined and there is a residual pillar with a width of 15 m. The width of the protective pillar under the residual pillar is 18m. Working face 21177 is located to the left of the pillar in coal seam #17; the distance between the haulage lane of 21177 and the edge of the pillar in face #14 is 15m. During mining operations, the deformation of the haulage lane of 21177 was small, with a horizontal deformation and vertical deformation of 265 and 183 mm, respectively. Working face 21177 is located to the right of the pillar and was the last working face along coal seam#17. To reduce the width of the coal pillar in seam #17, the distance between the 21178 return tunnel and the pillar edge was adjusted to 10m (the coordinates of the tunnel's central point R are (21.3, 20.1)). The 21178 return tunnel is arch shaped with a bottom width of 4.6 m, two ribs height of 0.8 m, and an arch radius of 2.3 m. The tunnel is supported by bolts. The parameters for the bolt assembly are as follows: the bolt diameter is 20 mm, bolt length is 2200 mm, tensile strength is 335 MPa, and bolt interval is 700 mm; the array pitch is 700 mm with 11 bolts per pitch and end anchoring. During excavation driving, the tunnel surface suffered significant deformation and the bolts and anchor on the roof near the pillar were broken. The grouting reinforcement had little effect on the deformation control and the safety of the excavation operation was severely impaired. The parameters of 21178 return tunnel as shown in Fig.8.

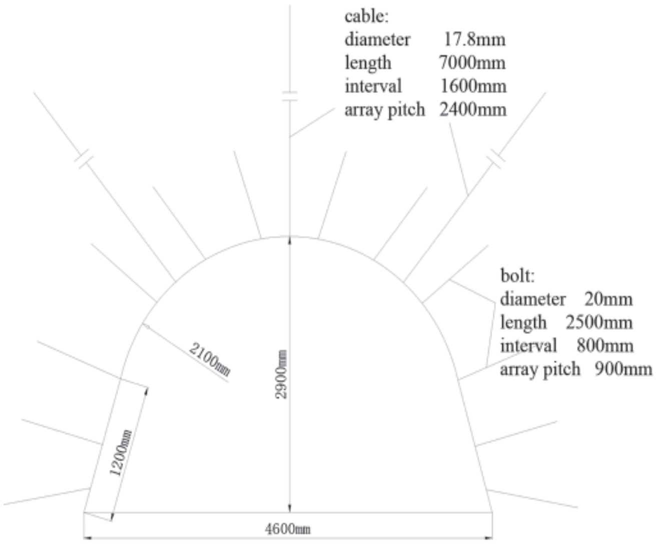

Fig.8 Tunnel shape and initial support parameters

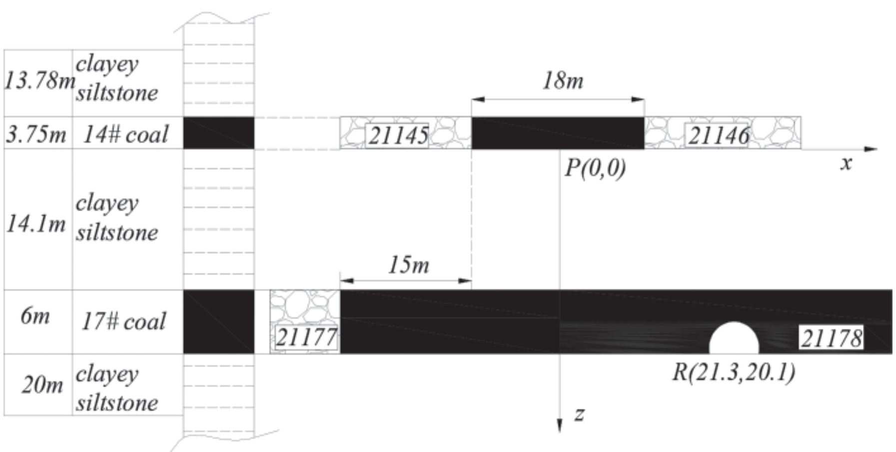

Fig.7 Cross section diagram showing the coal seams, mining faces, and return tunnel

3.2 Tunnel instability coefficient calculation and support optimization

We assume that the stress distribution on the pillar after the mining of working face 21146 was symmetric with that of the stress distribution after the mining of 21145. The stress distribution after the mining of 21145 was measured by a perforate stress gauge and is shown in Fig.9 (dashed line), along with the curve of the stress on the gob pillar (solid blue line).

The tunnel can be reduced to an arch-shaped tunnel for convenience.

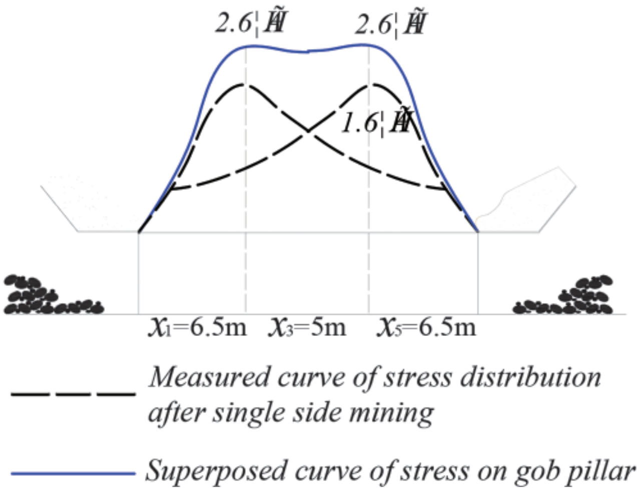

Fig.9 Curves showing the stress caused by mining and the stress on the gob pillar

The equivalent radius of the arched tunnel is 2.57m. The parameters of the 21178 return tunnel are shown in Table I.

TABLE I PARAMETERS OF 21178 RETURN TUNNEL

H/m	484	c^*/MPa	4.03
K_1	2.6	$\phi^*/°$	32.8
K_2	0	L/m	2.2
K_3	2.6	d/m	0.02
x_1	6.5	σ_b/MPa	335
x_2	0	μ	13
x_3	5	D_b/m	0.9
x_4	0	n	1.4
x_5	6.5	j	21.57
x_p/m	20	k	20.1
r/m	2.57		

Substituting the parameters in Table1 into Eq.(26), the tunnel instability coefficient, η, is 1.122 (i.e., the coefficient is greater than 1.0) which indicates that the 21178 return tunnel is unstable. Based on the tunnel instability coefficient, the reason for the large deformation of the tunnel can be concluded as follows: (1) the distance between the 21178 return tunnel and the upper pillar edge is small; therefore, the stress on the CRBBS exceeds the strength of the CRBBS. (2) The support structure is not strong enough to sustain the overhead stress. After analysing the damage mechanism, an optimization scheme that included adjustments to the bolt strength and bolt length was proposed: The bolt strength was adjusted from 335MPa to 500MPa and the length of the bolt was changed from 2.2m to 2.5m; at this point, η = 0.982 while the other parameters were fixed.

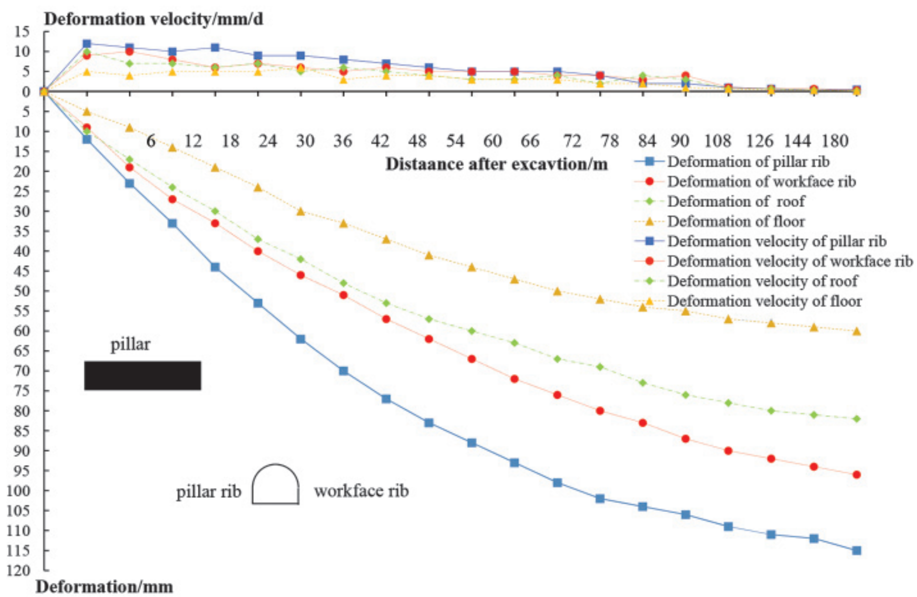

Fig.10 Deformation and velocity in the return tunnel after parameter optimization

3.3 Strata control observations

As a result of our study, the optimization scheme was imposed in the mine. During the excavation of the tunnel after supporting parameters optimization, the subsidence of the roof and convergence of the two sides were 82 mm and 211 mm, respectively. The subsidence of the pillar rib and the convergence of the working face rib were 115 mm and 96 mm, respectively (expressed as in Fig.10). These results demonstrate the effectiveness of the optimization scheme.

4. Discussion

Four methods are commonly used to evaluate or determine the safe position for a tunnel under a gob pillar: the pressure boundary method (Zhang et al., 2012; Xu et al., 2015), change rate of stress method (CRSM) (Zhang, 2008), and tunnel stability index method (TSIM) (Lu et al., 1993).

4.1 Outline of the four methods

(1) Pressure boundary method

In the abutment pressure boundary method (APBM) and deviator stress boundary method (DSBM), the tunnel is located outside the zone affected by the pillar load. Fig.11 illustrates the APBM. In the in homogeneous field caused by the gob-pillar stress, a stress of 0.1 σ_p is assumed to have no influence on the tunnel and is regarded to be the influence boundary. The tunnel should be located outside of the zone affected by the pillar load. DSBM, similar to APBM, sets a deviator stress boundary and places the tunnel beside the boundary. Here, for brevity we use APBM as an example.

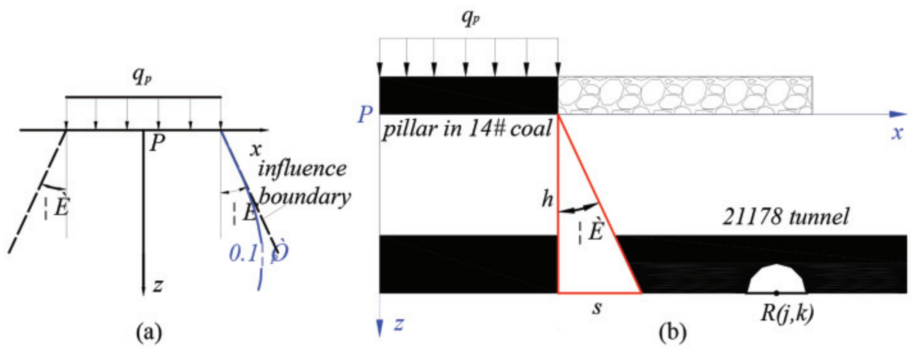

Fig.11 Diagram illustrating the APBM

$$K = \left| \frac{d\sigma_{(x)}}{dx} \right| \quad \text{... (29)}$$

where $\sigma_{(x)}$ is the stress distribution function in the pillar floor, and x is the horizontal distance between the edge of the pillar and the tunnel. Here, we assume that K = 0.22 is the critical value. The distance between the 21178 return tunnel and the pillar edge is 18.6m.

Based on APBM, the position of the tunnel can be described as

$$s > h\cot\theta \quad \text{... (27)}$$

where θ (22-55°) is the angle of the stress influence zone, θ increases as the abutment pressure increases, and the pillar width decreases.

For the conditions of the Huopu colliery, the influence angle is assumed to be 36°; then, the distance between the 21178 return tunnel and the pillar edge (denoted here as the 21178 distance) should be 14.6 m.

(2) TSIM

As shown in Eq.(28), the ratio of maximum pressure at the tunnel position before excavation (σ_{max}) over the uniaxial compressive strength (σ_c) is defined as the tunnel stability index (A). The relation between the stability level and tunnel stability index is shown in Table II. For the 21178 return tunnel, the maximum pressure at the tunnel position before excavation is 3.46 MPa and the uniaxial compressive strength is 7.38 MPa. Consequently, the tunnel stability index is 0.468, indicating instability. According to Eq.(21) and Eq. (28), the tunnel is stable only when the 21178 distance is more than 20m.

$$A = \frac{\max\left\{\sigma^{P}{}_{x}, \sigma^{P}{}_{y}\right\}}{\sigma_c} \quad \text{... (28)}$$

TABLE II SURROUND ROCK STABILITY LEVEL

Stability level	Tunnel stability index *(A)*
Stability	<0.25
Middle stability	0.25~0.4
Instability	0.4~0.65

(3) CRSM

When determining the influence of the support structure for a tunnel located close to the coal seam, the extent of the stress inequality is as significant as the position of the tunnel beside the zone affected by the pillar load. The inequality extent can be evaluated by the change in stress along the x direction:

(4) Tunnel instability coefficient method (TICM)

Through TICM, the changes in the stress distribution and the strength reinforcement by the bolts is quantified. According to Eq.(26), the horizontal coordinate of the tunnel centre is 23.7 while the tunnel instability coefficient is fixed to 1 and the vertical distance between the 21178 return tunnel and pillar floor is 20.1; thus, the 21178 distance is 12.4m.

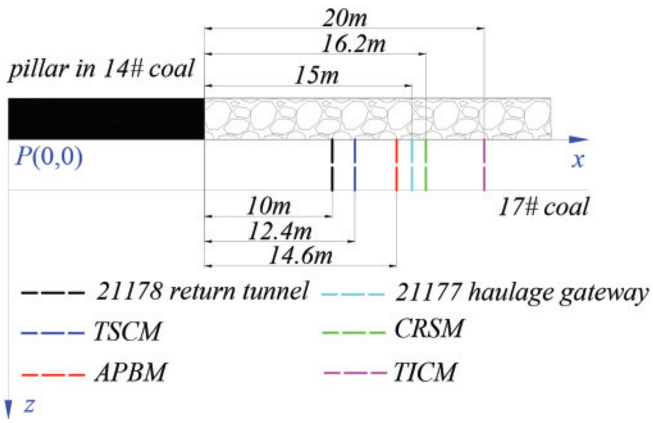

Fig.12 Comparison of the optimal '21178 distance' calculated by TSCM, CRSM, APBM, and TICM

4.2 Discussion

The 21178 distance calculated by the four methods (Fig.12) was compared to current locations of the 21178 return tunnel and the 21177 haulage gateway. The geo-engineering conditions of the 21177 haulage gateway are similar to those of the 21177 return tunnel except for the distance between each tunnel and the pillar edge, resulting in different deformation control effects: there is less deformation in the 21177 haulage gateway (21177 distance 15m) compared to the deformation near the 21178 return tunnel (21178 distance 10m).

The 21178 distance calculated by APBM is 14.6m, which is close to the current position of the 21177 haulage gateway; thus, the APBM result is in agreement with the 21178 return tunnel location. However, the value of the influence angle is determined empirically and therefore contains an uncertainty. While the 21178 distances determined by TSCM and CRSM have a higher safety factor and are both large than 15 m, the loss of coal is also higher. The stress boundary and the extent of stress inequality are both considered in CRSM, but the relation between the stress changes and tunnel stability was not discussed in Xu (2015).

The 21178 distance assigned by TICM is 12.4m, which may lead to tunnel damage, since at this distance the stress on the CRBBS exceeds the CRBBS strength. TICM can be seen as a combination of APBM and TSCM. As the reinforcement of bolts is considered, the strength of the structure consisting of the surrounding rock and the bolts is quantified. Therefore, the result produced byTICM is more practical and it is easier to control the pillar width of the lower coal seam. Moreover, TICM can be used to evaluate the stability of existing tunnels and to design support optimization. However, as this method has many inadequacies in optimal matching of the tunnel position with the support parameters, this method could be improved by combining it with a mathematical model of optimal selection.

5 Conclusions

Combined with the Weibull distribution function, we modified the calculation formula of the strength of a CRBBS and the calculation formula of the stress distribution of the tunnel CRBBS under a load from the upper pillar. The radial stress within the CRBBS under an inhomogeneous stress field caused by a residual pillar is calculated.

The tunnel instability coefficient (η) is derived to quantitatively describe the relationship among the tunnel position, tunnel parameters, support parameters, and the rock mechanical properties. The value of the coefficient is the ratio of the maximum radial stress within the CRBBS to the strength of the CRBBS; the CRBBS is stable only when $\eta < 1$. Using the tunnel instability coefficient, the stability limit condition of the 21178 return tunnel is estimated as a guide for the optimization of the support parameters. As a result, the large deformation of the 21178 return tunnel is controlled.

According to TICM, the optimum distance between the 21178 return tunnel and the pillar edge is 12.4 m; thus, the current 21178 distance (10m) is not large enough to prevent damage to the tunnel. The proposed method is verified by comparing its results with those calculated by three other methods. As the resistance from the bolt to the inhomogeneous stress field is calculated, the tunnel position evaluated by the tunnel instability coefficient is more accurate.

Acknowledgements

This paper is supported by “Priority Academic Program Development of Jiangsu Higher Education Institutions,” and “the Fundamental Research Funds for the Central Universities (2017XKQY044)”.

Reference

1. Cheng L., Zhang, Y.D., Ji, M., Cui, M.T., Zhang, K., and Zhang, M.L. (2015): Theoretical calculation and analysis on the composite rock-bolt bearing structure in burst-prone ground. *Mathematical Problems in Engineering*. Vol.2015, No.21, pp. 1-6.
2. Cheng, L.K. and Fan, J.L. (2003): Geotechnical Anchorage. *China Architecture& Building Press.* pp. 60-61.
3. Fang, Y., Xu, C., Cui, G., and Kenneally, B. (2016): Scale model test of highway tunnel construction underlying mined-out thin coal seam. *Tunnellingand Underground Space Technology.* Vol.56, pp. 105-116.
4. Hou, C.J. (2013): Ground Control of Roadways. *China University of Mining and Technology Press.* pp. 130-156.
5. Kang, Q.R., Tang, J.X., Hu, H., and Zhang, W.Z. (2011): Stress distribution rule of roadway affected by overhead mining in gently inclined coal seams group. *Transactions of Nonferrous Metals Society of China.* Vol.21, No.S3, pp. s529-s535.
6. Li, J.T. and Cao, P. (2005): Catastrophe analysis on pillar instability considered mining effect. *Journal of Central South University.* Vol.12, No.1, pp. 102-106.
7. Liu, X., Li, X., and Pan, W. (2016): Analysis on the floor stress distribution and roadway position in the close distance coal seams. *Arabian Journal of Geosciences.* Vol.9, No.2, pp. 1-8.
8. Lu, S.L., Sun, Y.L., and Jiang, Y.D. (1993): Determination of horizontal distance between tunnel and upper coal seam. *Journal of China University of Mining & Technology.* Vol.22, No.2, pp. 1-7.
9. Mathey, M. and van der Merwe, J.N. (2016): Critique of the South African squat coal pillar strength formula. *Journal of the Southern African Institute of Mining and Metallurgy.* Vol.116, No.3, pp. 291-299.
10. Suchowerska, A.M., Merifield, R.S., and Carter, J.P. (2014). Vertical stress changes in multi-seam mining under supercritical longwall panels. *International Journal of Rock Mechanics & Mining Sciences.* Vol.70, No.7, pp. 240-251.
11. Shang, Y.J., Li, K., He, W., and Sheng, C. (2014): From the new Austrian tunneling method to the geoengineering condition evaluation and dynamic controlling method. *Journal of Rock Mechanics and Geotechnical Engineering.* Vol.6, No.4, pp. 366-372.
12. Tan, Y.L., Zhao, T.B., and Xiao, Y.X. (2010): In situ investigations of failure zone of floor strata in mining close distance coal seams. *International Journal of Rock Mechanics & Mining Sciences.* Vol.47, No.5, pp. 865-870.

13. Wilson, A.H. (1983): The stability of underground workings in the soft rocks of the coal measures. *Geotechnical and Geological Engineering.* Vol.1, No.2, pp. 91-187.

14. Xu, L., Wei, H.X., Xiao, Z.Y., and Li, B. (2015): Engineering cases and characteristics of deviatoric stress under coal pillar in regional floor. *Rock and Soil Mechanics*. Vol.36, No.02, pp. 561-568.

15. Xie, S.R., Sun, Y.J., He, S.S., Li, E.P., Gong, S., and Li, S.J. (2016). Distinguishing and controlling the key block structure of close-spaced coal seams in China. *Journal of the Southern African Institute of Mining and Metallurgy.* Vol.116, No.12, pp. 1119-1126.

16. Yan, H., Weng, M.Y., Feng, R.M., and Li, W.K. (2015): Layout and support design of a coal road way in ultra-close multiple-seams. *Journal of Central South University.* Vol.22, No.11, pp. 4385-4395.

17. Yang, J.X., Liu, C.Y., Yu, B., and Wu, F.F. (2015): Calculation and analysis of stress in strata under gob pillars. *Journal of Central South University.* Vol.22, No.3, pp. 1026-1036.

18. Yang, Z.F. (2013): Two challenging issues worth of attentions in engineering geology nowadays. *Journal of Engineering Geology.* Vol.21, No.4, pp. 481-486.

19. Zhao, J.L. and Fu, Q. (1998): New scheme of roadway layout in longwall top-coal caving system. *International Journal of Mining Science and Technology.* Vol.70, No.2, pp. 162-165.

20. Zhang, W., Zhang, D.S., Chen, J.B., Wang, X.F., and Xu, M.T. 2012. Determining the optimum gateway location for extremely close coal seams. *Journal of China University of Mining & Technology.* Vol.41, No.2, pp. 182-188.

21. Zhang, B.S., Yang, S.S., Kang, L.X., and Zhai, Y.D. (2008). Discussion in method for determining reasonable position of roadway for ultra-close muti-seam. *Chinese Journal of Rock Mechanics and Engineering.* Vol.27, No.01, pp. 97-101.